Cure Kinetics of a Low Epoxide/Hydroxyl Group-Ratio Bisphenol A Epoxy Resin–Anhydride System by Infrared Absorption Spectroscopy

GARY C. STEVENS, *Central Electricity Research Laboratories, Leatherhead, Surrey, KT22, 7SE, United Kingdom*
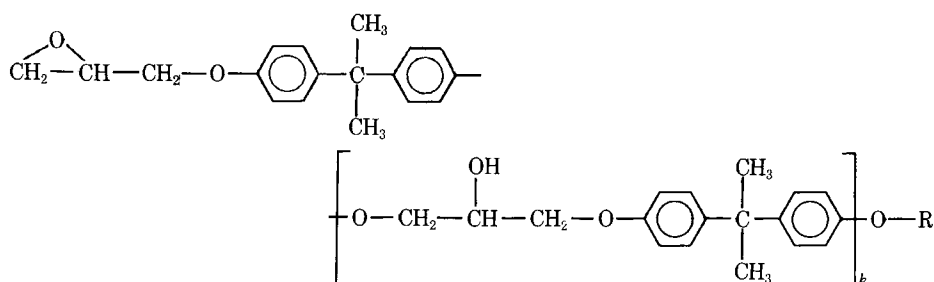
Synopsis

An infrared absorption spectroscopy study of the curing kinetics of a low (1.12) epoxide/hydroxyl-group ratio bisphenol A epoxy resin–phthalic anhydride system is reported. A full infrared peak assignment to molecular vibrational modes is given for the range 400 to 4000 cm^{-1}, and the optical density behavior of all peaks during reaction is discussed in detail. Proposed rival reaction mechanisms are considered and their respective kinetic behavior discussed. The reaction was found to follow consecutive-step addition esterification and simultaneous addition etherification, and epoxide–hydroxyl group and carboxylic acid dimer hydrogen bonding was found to occur. The reaction behavior supports a proposed hydroxyl group-limited inhomogeneous bulk reaction mechanism of a colloid type.
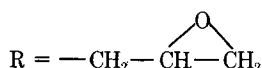
INTRODUCTION

In an effort to understand the chemical and morphological nature of anhydride-cured bisphenol A type epoxy resins and elucidate chemical structure–morphology–physical property relationships, a comprehensive chemical and structural investigation of two technologically important systems has been initiated. Spectroscopic and light scattering studies of one system prior to and during reaction have been briefly reported, and an inhomogeneous reaction mechanism has been proposed.[1] Several authors have studied the reaction mechanism of epoxy systems with and without catalysts and diluents and in the presence of anhydrides using wet chemical analysis methods.[2–5] However, model epoxide compounds and differing epoxy resin types and anhydrides have been used and conflicting reaction mechanisms and kinetics have been reported.[2,3] The need to undertake correlation tests of chemical structure and reaction behavior with light scattering behavior and microstructure and electrical, mechanical, and thermal properties required a reassessment of the reaction mechanism for the systems under consideration. This was also necessary because light scattering quality materials were prepared involving impurity removal which could influence or confuse the reaction mechanism.

Infrared absorption spectroscopy was chosen to avoid the inherent difficulties in reliable functional group analysis particularly beyond the gel point and to provide a general probe for intermediate structures and intermolecular interactions. However, as discussed below, a number of disadvantages result, but these are tolerable.
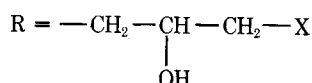
The systems of interest are based on the diglycidlyl ether of bisphenol A (DGEBA) structure:

CCC 0021-8995/81/124259-20$02.00

$$CH_2-CH-CH_2-O-\underset{CH_3}{\overset{CH_3}{C}}-$$

$$\left[\begin{array}{c}OH\\O-CH_2-CH-CH_2-O-\underset{CH_3}{\overset{CH_3}{C}}-O-R\end{array}\right]_k$$

where the diepoxide oligomers contain

$$R = -CH_2-CH-CH_2$$

Some endgroup impurity oligomers of the type

$$R = -CH_2-\underset{OH}{CH}-CH_2-X$$

may also be present giving chlorohydrin (X = Cl) and α-glycol (X = OH) structures. The two systems under study are produced by Ciba–Geigy under the product code CT200–HT901 and CY207–HT903, where HT components are anhydride compounds. The epoxy resin components are multioligomeric exhibiting k values up to 12. The average value of k for CT200 is about 1.7, and that for CY207 is about 0.36. Characterization of the systems actually used, by functional group analysis and gel permeation chromatography, yields the structural information summarized in Table I. The CT200 system is seen to

TABLE I
Structural and Reaction Condition Comparison of the Bisphenol A Epoxy Resin–Anhydride Epoxy Resin Systems CT200–HT901 and CY207–HT903[a]

Variable	CT200	CY207
Epoxide content, mol/kg[b]	2.4 ± 0.1	4.5 ± 0.1
Hydroxyl content, mol/kg[c]	2.1–2.2	0.7–1.2
Epoxide/hydroxyl molar ratio	1.12	4.74
Bisphenol A resin mass fractions, %[d]		
$k = 0$	15.4	61.2
1	18.4	10.2
2	14	5.8
3	13.7	2.6
4	10.6	2.7
$k > 4$	19.3	8.4
$k = 0$ α-Glycol	3.5[e]	8.8
or chlorohydrin	3.7[e]	9.2
	CT200-HT901	CY207-HT903
Resin/hardener mass ratio	3.33	1.66
Epoxide/anhydride molar ratio	1:0.85	1:0.91
Gelation temperature, K	—	353
Cure temperature, K	398	393

[a] PA = Phthalic anhydride, THPA = tetrahydrophthalic anhydride.
[b] Determined by potassium iodide method.[4]
[c] Inferred from GPC data; endgroup impurity possibilities account for the range.
[d] Calculated assuming α-glycol endgroup impurities.
[e] CT200 $k = 0 + 1$ give 8.25% and 8.55% for α-glycol and chlorohydrin endgroups, respectively.

be representative of a Taffy process resin[6] containing a low-integral epoxide/hydroxyl group ratio, whereas the CY207 stem represents a high epoxide/hydroxyl group system controlled largely by its $k = 0$ fraction. The temperature dependence of the ν_{O-H} infrared peak in the unreacted CT200 system compared with the CY207 system indicates stronger free hydroxyl-group hydrogen bonding in the former. Light scattering observations[1] support a heterogeneous, temperature-dependent resin structure, and the formation of molecular aggregates dependent on hydroxyl–epoxide group hydrogen bonding has been proposed.[1]

This report will deal with the curing behavior of CT200–HT901 under the conditions summarized in Table I. The following report will deal with the other system complementing the interpretation of reaction mechanism.

POSSIBLE REACTION SCHEMES

Two principal groups of investigators have dealt with the reaction mechanism of anhydride-cured epoxy resins, and general reviews are available.[4,5] Others have dealt with both base- and acid-catalyzed reactions of model compounds.[7-9]
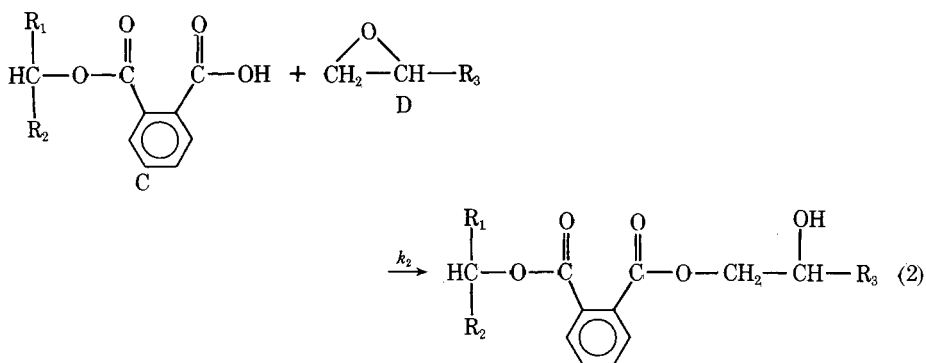
Fisch and Hofmann[2] proposed the following step addition reactions to account for the three-dimensional crosslinked nature of the matrix and functional group behavior in the absence of catalysts.
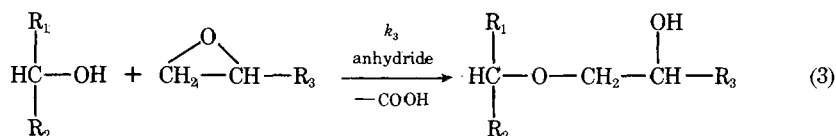Addition Esterification:

<div align="center">monoester formation:</div>

$$\text{(1)}$$

<div align="center">diester formation</div>

$$\text{(2)}$$

Addition Etherification:

$$\text{(3)}$$
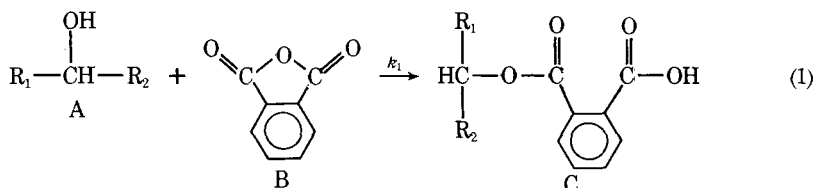
In this scheme, phthalic anhydride reacts with a resin chain or endgroup free hydroxyl group to generate a monoester linkage and a carboxylic acid group, reaction (1). The carboxylic acid group may then react with a terminal epoxide group to form an hydroxy diester linkage, reaction 2. To account for excess epoxide consumption, homopolymerization in the presence of carboxylic acids or anhydrides was considered a competing reaction, reaction 3. Condensation reactions were considered negligble. Reactions (2) and (3) regenerate free hydroxyl groups which are potentially available for further reaction. If reactions (1) and (2) go to completion, the free hydroxyl content should be conserved.

Tanaka and Kakiuchi[3] considered different epoxy systems and found that the anhydride and epoxide consumption rates paralleled each other and that etherification was minimal up to the gel point. This led to the proposal of a termolecular reaction scheme via an activated complex such that

$$\tag{4}$$
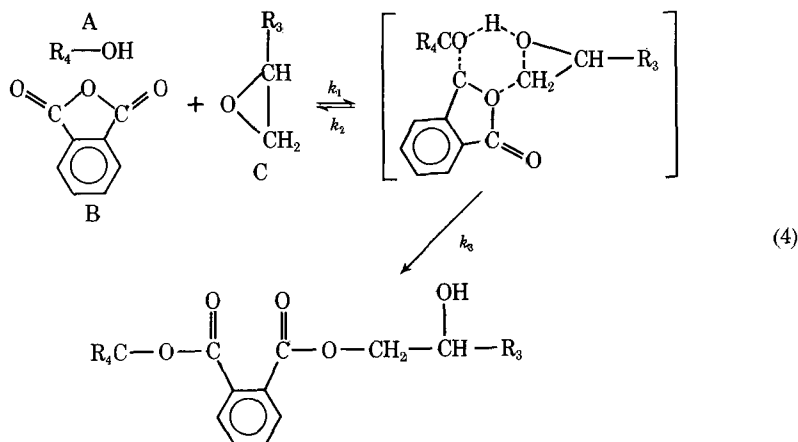
In this case, if the lifetime of the activated complex is short, the free hydroxyl group content will be continuously conserved, whereas reaction (1) acts as a sink. However, this scheme was considered of low probability due to the large negative activation entropy required. Therefore, an alternative but kinetically indistinguishable scheme was proposed:

$$\tag{5}$$

$$\tag{6}$$
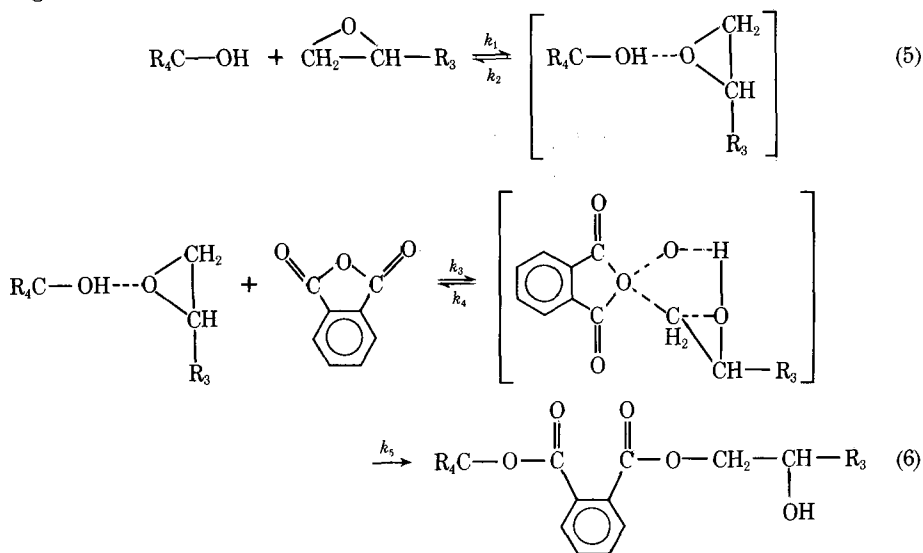
The inclusion of hydroxyl–epoxide group hydrogen bonding and concomitant local ordering prior to reaction lowers the excess negative entropy required. This is clearly relevant to the hydrogen bonding present in the system considered here. A common feature of reactions (4), (5), and (6) is the absence of carboxylic acid structures in contrast with reaction (1).

Reaction Kinetics

Tanaka and Kakiuchi have modeled the kinetics of their schemes such that for time-dependent activated complex concentration, the termolecular reaction velocity V is given by

$$V = -\frac{d[B]}{dt} = K[A][B][D] \tag{7}$$

where the compound rate constant K simplifies to $k_1 k_3/(k_2 + k_3)$ for reaction (4) and to $k_1 k_2 k_5/(k_2 k_4 + k_2 k_5)$ for reactions (5) and (6). Thus, if all groups are equally available, anhydride consumption and diester formation are third-order reactions.

Fisch and Hofmann did not kinetically model their scheme. Applying simple reaction rate considerations necessitates inclusion of the regenerated free hydroxyl groups such that for reactions (1) to (3),

$$A + B \xrightarrow{k_1} C \tag{8}$$

$$C + D \xrightarrow{k_2} E(A') \tag{9}$$

$$A + D \xrightarrow[B, C]{k_3} F(A') \tag{10}$$
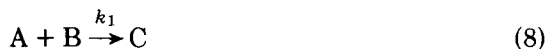
Equations (8) to (10) represent a set of coupled simultaneous reactions whose corresponding set of differential equations is analytically insoluble. However, for CT200–HT901, $[A] \simeq [B] \simeq [C]$; and anhydride consumption, represented by $\dot{B} = k_1 [A][B]$, will appear second-order during the initial phase of reaction. However, if hydroxyl group or anhydride availability is restricted, pseudo first-order kinetics may be expected. This will also be the case for the Tanaka and Kakiuchi schemes.

Equations (8) and (9) represent consecutive-step reactions such that neglect of the regenerated hydroxyl group coupling term (A') allows a comparison with the consecutive first-order reaction sequence:

$$M_1 \xrightarrow{k_{12}} M_2 \xrightarrow{k_{23}} M_3 \tag{11}$$
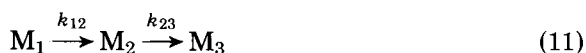
which provides a simple analytic solution.[10] In this case, M_1 follows simple first-order kinetics and M_2 undergoes peaking and M_3 displays S-shaped behavior with an induction period such that both are dependent on k_{12} and k_{23}.

Thus, the schemes of Fisch and Hofmann and Tanaka and Kakiuchi present a number of distinct differences with respect to product and intermediate chemical structure and reaction kinetics, and these may be investigated.

EXPERIMENTAL

CT200 and HT901 were repeatedly filtered through 0.2 μm PTFE filters at elevated temperatures in dry nitrogen under pressure to remove dust and particulate matter including dicarboxylic acid impurities in the HT901 (phthalic anhydride) component. The phthalic anhydride (PA) was recrystallized between filtrations. CT200 was subsequently exhaustively stirred and evacuated at 393 K to degas and remove volatile impurities, which were principally water and oxygenated solvents. A CT200/HT901 reactant mass ratio of 100:30 was used as recommended by Ciba–Geigy. This corresponds to an epoxide:anhydride molar stoichiometry of 1:0.85, an optimum stoichiometry for this type of system.[4] To achieve rapid mixing, the reactants were mixed in the liquid phase followed by exhaustive stirring and partial degassing at 398 K. Sample volumes of 4 to 10 ml were cured in closed glass bottles at the recommended temperature of 398 K, and at prescribed times individual samples were cooled to room temperature prior to spectral recording.

Early experiments, in which capillary films of CY207–HT903 between KBr discs were cured in situ, produced similar spectral changes to those to be described, but the reaction rates were an order of magnitude higher and inconsistent with light scattering parameter, density, glass transition, and other rate of change parameters. This was clearly present in the work of Lüttgert and Bonart,[11] but they did not recognize the disparity. KBr or surface-absorbed water may be responsible. Alternatively, a thin film undergoing inhomogeneous reaction could produce an apparent rapid reaction rate.

As cure progresses, the material transforms from a liquid to a crosslinked solid, and infrared sample preparation involved two options. If samples could not form capillary films between KBr discs below a preparation temperature of 350 K, they were ball milled to a fine powder, mixed with dry KBr powder, and a transmission disc obtained by pressing. These spectra were checked by the Nujol Mull method also. However, ball milling made the free hydroxyl absorptions unreliable due to absorbed water. Spectra were recorded at room temperature on a Perkin–Elmer 577 spectrometer adopting standard methods. Wave number calibration was against a polystyrene film, and peak optical densities

$$D_i = \log \frac{I_i^0}{I_i^T} = \epsilon_i C_i L \qquad (12)$$

were determined by consistent baseline interpolation.[12] Reliable extinction coefficient (ϵ_i) data are not available, so optical density was used to follow the reaction behavior assuming a constant ϵ_i for any absorption i. Correctly referenced optical densities were obtained by comparing the optical density of every peak (i) in a particular spectrum (j) to its corresponding peak in a reference spectrum (r) to obtain a normalization factor for each peak:
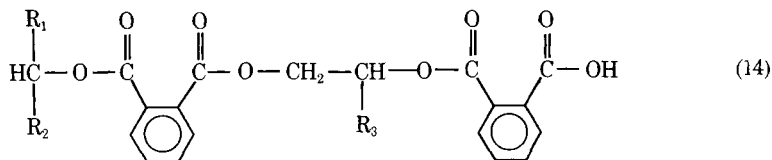
$$k_{j,r}^i = \frac{D_{j,i}}{D_{r,i}} \qquad (13)$$

Those peaks associated with unchanging chemical groups were noted allowing several reliable reference peaks to generate a mean normalization factor $\langle k_{j,r} \rangle$ for the complete spectrum in question.
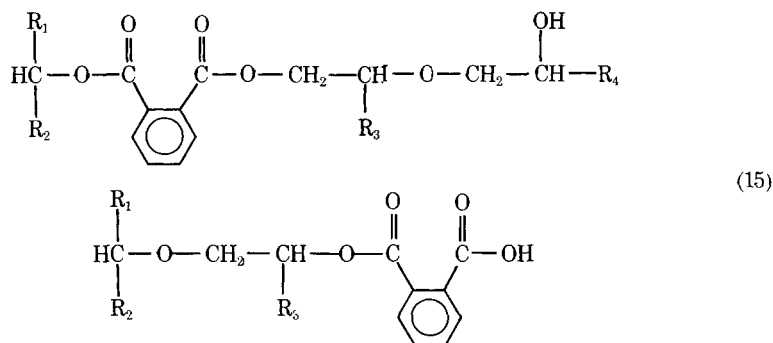
INFRARED PEAK ASSIGNMENTS AND OPTICAL DENSITIES

During reaction, the product structures of reactions (1) to (6) could occur. Further reactions involving the above product structures could lead to additional structures including:
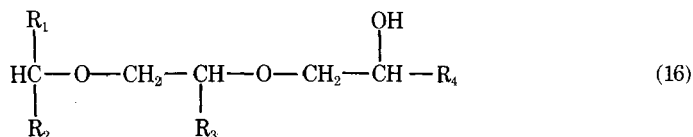
Polyester Linkages:

$$\underset{R_2}{\overset{R_1}{\text{HC}}}-\text{O}-\underset{\text{O}}{\overset{\text{O}}{\text{C}}}\overset{\text{O}}{\underset{}{\text{C}}}-\text{O}-\text{CH}_2-\underset{R_3}{\text{CH}}-\text{O}-\underset{}{\overset{\text{O}}{\text{C}}}\overset{\text{O}}{\underset{}{\text{C}}}-\text{OH} \tag{14}$$

Ester–Ether Linkages:

$$\underset{R_2}{\overset{R_1}{\text{HC}}}-\text{O}-\overset{\text{O}}{\text{C}}\overset{\text{O}}{\text{C}}-\text{O}-\text{CH}_2-\underset{R_3}{\text{CH}}-\text{O}-\text{CH}_2-\overset{\text{OH}}{\text{CH}}-R_4$$

$$\underset{R_2}{\overset{R_1}{\text{HC}}}-\text{O}-\text{CH}_2-\underset{R_5}{\text{CH}}-\text{O}-\overset{\text{O}}{\text{C}}\overset{\text{O}}{\text{C}}-\text{OH} \tag{15}$$

Polyether or Branched Ether Linkages:

$$\underset{R_2}{\overset{R_1}{\text{HC}}}-\text{O}-\text{CH}_2-\underset{R_3}{\text{CH}}-\text{O}-\text{CH}_2-\overset{\text{OH}}{\text{CH}}-R_4 \tag{16}$$

Consideration of these final and intermediate structures aids assignment of those peaks arising during reaction.

The detailed peak assignments of the unreacted bisphenol A epoxy resin are listed in Table II, and the reacting resin–phthalic anhydride peak assignments and optical density ranges are shown in Table III. In the latter, spectral normalization included the use of the following resin peaks: 2962, 1605, 1580, 1382, 1360, and 830 cm^{-1}. Extensive use was made of infrared structural correlation tables[13] and literature sources including the work of Hase et al. on phthalic anhydride[14] (their vibrational mode nomenclature is used here), Sidyakin et al. on radiation reactions in epoxide oligomers,[15] Sidyakin[16] and Eyerer[17] on amine-cured epoxide resins, and Komarova[18] on the interaction of polyesters with epoxy polymers.

Figure 1 illustrates three spectra obtained at different reaction times showing the significant changes which occur. Table III tabulates the peak assignments and their corresponding optical density value or range with respect to a reference spectrum obtained at the start of cure. Some of the more minor peaks in Table II are not dealt with in Table III.

In the unreacted CT200 resin, the free hydroxyl $\nu_{\text{O--H}}$ peak is a doublet with

TABLE II
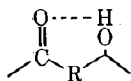DGEBA Infrared Spectral Peak Assignments

Peak or band, cm^{-1}	Assignment
3450–3500	νO–H
3050	Aromatic C—H stretch
3038	Epoxide CH, C—H
2998	Epoxide methylene C—H
2928	Ether methylene C—H assym. stretch
2840	Ether methylene C—H sym. stretch
2872	Methyl C—H sym stretch
2962	Methyl C—H assym. stretch
1700–2200	Aromatic combination bands
1605	
1580	
1508	Aromatic C=C bands
1560	
1430	Epoxide $\delta_{C—H}$
1410	Epoxide/ether $\delta_{C—H}$
1382	Methyl $\delta_{C—H}$ sym. defeformation
1360	Ether methylene $\delta_{C—H}$
1345	Epoxide methylene $\delta_{C—H}$
1290–1310	γ_{CH_2}, aromatic $\delta_{C—H}$, $\delta_{—OH}$
1230–1260	Aromatic ether aryl C—O, epoxide C—O—C
1185	Aromatic $\delta_{C—H}$ (in plane)
1105–1135	Aromatic $\delta_{C—H}$, C(CH$_3$)$_2$ skeletal
1038	Aromatic $\delta_{C—H}$, aromatic ether alkyl C—O
1010	Aromatic $\delta_{C—H}$
915–920	Epoxide deformation
862	Epoxide deformation
830	Aromatic $\delta_{C—H}$ out-of-plane
810	C(CH$_3$) skeletal
750–780	CH$_2$ skeletal
Lower peaks	Assignment unclear

peak contributions at 3450 and 3500 cm^{-1} due to the presence of two distinct H-bonded hydroxyl species. This doublet remained during cure; but during the early phase of cure, the whole doublet is shifted by 50 cm^{-1} to higher frequencies characteristic of a reduction of H bond strength. Also, the $\nu_{O—H}$ peak optical density for several unreacted CT200 spectra referenced with respect to the cure values of the 2962, 1605, 1508, 1038, and 830 cm^{-1} peaks gave a "before cure" value of 0.0548 ± 0.0036, whereas during the first 3 h of cure when the ν_{O-H} optical density appeared constant, a value of 0.0503 ± 0.0028 was obtained.

Immediately on reaction, broad spectral features appeared around 3000 and 2550 cm^{-1} which increased and peaked during cure. Following IRSCOT and Patterson and Ward[19] and Ward,[20] these were assigned to carboxylic acid group H-bonded dimer structures:

$$R_1—C\overset{OH\text{-}\text{-}O}{\underset{O\text{-}\text{-}HO}{}}C—R_2$$
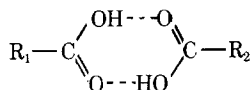
The 3000 cm^{-1} peak arises from a $\nu_{O—H}$ mode, and the 2550 cm^{-1} peak is considered a $\nu_{C—O}$, $\delta_{O—H}$ combination mode. These peaks were clearly present in the infrared spectrum of 4-cyclohexane-1,2-dicarboxylic acid. Intramolecular chelate structures of the form

may also contribute to these bands.

TABLE III
CT200–HT901 Infrared Spectral Peak Assignments and Optical Density Variation During Reaction

| Peak, cm^{-1}	Assignment	Optical density
3500	ν_{O-H}	0.0548
		Step change to 0.0503
3000	Associated acid	0 step to 0.061
	ν_{O-H}	$0.061 \rightarrow 0.0045$
2550	Associated acid	
	ν_{C-O} and δ_{O-H}	$0 \rightarrow 0.024 \rightarrow 0.016$
	combination	
2962	Methyl ν_{C-H} asymmetric stretch	0.125
1850	P.A. $\nu_{C=O}$	$0.215 \rightarrow 0.015$
1802	P.A. $2\nu_{35}$	$0.04 \rightarrow 0$
1788	P.A. $\nu_9 + \nu_{37}$ combination	$0.23 \rightarrow 0.01$
1772	P.A. $\nu_{C=O}$	$0.35 \rightarrow 0.02$
1725	Aromatic ester $\nu_{C=O}$	$0 \rightarrow 0.3$
1705	Carboxylic acid $\nu_{C=O}$	Too weak
1605		0.164
1580	Aromatic (bisphenyl)	0.08
1508	$\nu_{C=C}$ bands	0.398
1460		0.096
1468	P.A. ν_{C-C}	$0.12 \rightarrow (\sim 0)$
1410	Epoxide/ether δ_{C-H}	0.023
1382	Methyl δ_{C-H} symmetric	0.032
1360	Ether methylene δ_{C-H}	0.048
1430	Epoxide δ_{C-H}	
1345	Epoxide methylene δ_{C-H}	Too weak
1292	γ_{CH_2}, aromatic δ_{C-H} alcohol	0.11
	δ_{O-H}, carboxylic ν_{C-O}	
1257	P.A. ν_{C-O-C}	$0.4 \rightarrow 0$
	Epoxide ν_{C-O-C}	(Not deconvoluted)
1245	Aromatic ether aryl ν_{C-O}	0.42
1182	Aromatic (bisphenyl) δ_{C-H} in-plane	0.196
1140		$0.04 \rightarrow 0.115$
1120	Branched ether	$0.02 \rightarrow 0.12$
1068	ν_{C-O-C}	$0.03 \rightarrow 0.11$
1105	P.A. Aromatic δ_{C-H} bisphenyl	$0.072 \rightarrow 0.026$
	δ_{C-H}, $C(CH_3)_2$ skeletal	$\rightarrow 0.068$
	branched ether	
1038	Aromatic δ_{C-H}	0.143
	Aromatic ether alkyl ν_{C-O}	
1010	Aromatic δ_{C-H}	0.70
990	Ester γ-skeletal	$0 \rightarrow 0.05$
960		$0.008 \rightarrow 0.021$
936	Carboxylic δ_{-OH}	$0 \rightarrow 0.015$
900	P.A. ν_{C-O}, epoxide γ-ring	$0.25 \rightarrow 0.01$
862	Epoxide γ-ring	Too small
830	Aromatic bisphenyl δ_{C-H} out-of-plane	0.216
740	(Ester skeletal mode)	$0 \rightarrow 0.085$
712	P.A. γ_{C-H}	$0.225 \rightarrow 0.025$
534	P.A. $\delta_{(C-C-C)}$	$0.048 \rightarrow 0.02$

^{a} P.A. = Phthalic anhydride.
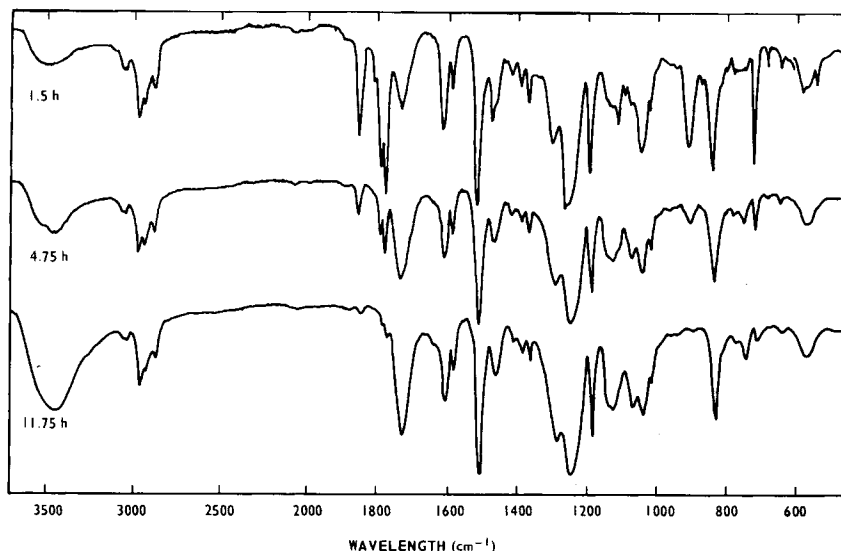
Fig. 1. Infrared spectral changes during the reaction of CT200–HT901 at 125°C. Spectra recorded at room temperature.

The 2962 cm^{-1} peak characterized the group of ν_{C-H} modes contributing in this region and summarized in Table II. Assignment here of the 3038 cm^{-1} peak to the epoxide–CH ν_{C-H} mode and the 2998 cm^{-1} peak to the epoxide–methylene (–CH$_2$) ν_{C-H} mode is considered correct as these features decrease during cure in line with anhydride consumption. Consequently, the aromatic ν_{C-H} peak at 3050 cm^{-1} sharpens considerably.

Following Hase et al.,[14] the 1850, 1802, 1788, and 1772 cm^{-1} peaks were assigned to the phthalic anhydride modes noted in Table III. All, as expected, decreased during cure.

During cure, a peak at 1725 cm^{-1} and a weak wing at 1705 cm^{-1} develop. The former is assigned to an aromatic ester $\nu_{C=O}$ mode and the latter to a carboxylic acid $\nu_{C=O}$. In this region and up to 2200 cm^{-1}, a number of weak resin–aromatic combination bands are also present.

The frequencies and intensity ratios of the next four peaks at 1605, 1580, 1508, 1460 cm^{-1} allow their assignment to the combined stretching and deformation aromatic $\nu_{C=C}$ bands. Contributions from resin methyl δ_{C-H} modes to the 1460 cm^{-1} peak may also be expected: the asymmetric mode in the 1430 to 1470 cm^{-1} region and the symmetric mode in the 1370 to 1380 cm^{-1} region. The 1468 cm^{-1} peak is assigned to the phthalic anhydride ν_{C-C} mode, and it decreased during cure.

The 1430 and 1345 cm^{-1} peaks by comparison with the CY207 spectrum can be assigned to epoxide group–CH$_2$ and –CHδ_{C-H} modes. The 1410 cm^{-1} peak decreases during cure, but its origin is uncertain; it may receive contributions from both epoxide and ether δ_{C-H} modes.

The 1292 cm^{-1} peak is likely to receive contributions from alcohol δ_{O-H}, carboxylic ν_{C-O}, and ether γ_{CH_2} modes. The most likely is unknown and the peak intensity variation during cure unreliable, so no definitive optical density data are discussed; at the start of cure, a value of 0.11 was obtained.

The 1257 cm^{-1} peak is one of three possible anhydride ν_{C-O-C} vibrations of which the middle band is missing or weak and the other occurs at 900 cm^{-1}. Both decrease during cure. The epoxide ν_{C-O-C} also occurs in this region but is not clearly discerned. The ν_{C-O} bands of aromatic ethers also fall in this region, and the 1245 cm^{-1} peak is assigned to the aryl–C—O bond ν_{C-O}. The associated alkyl bond ν_{C-O} frequency varies according to the nature of the alkyl group. In our case, contributions to the 1038 cm^{-1} peak are expected from the resin structure.

The 1182 cm^{-1} peak most likely results from the "1200 cm^{-1} band" of the aromatic δ_{C-H} (in plane deformations) where five other weak band contributions may be expected around 1150, 1105, 1090, 1030, and 980 cm^{-1}. These, together with other likely contributions, are listed in Table III.

During cure, peaks at 1140, 1120, and 1068 cm^{-1} appear and increase. The 1150 cm^{-1} region should receive aromatic δ_{C-H} contributions, and in general it is not well defined. Branched ether or polyether structures would account for these peaks best according to IRSCOT and the work of Davidson[21] on poly-ethylene glycol, $\left(\!(CH_2)_2\!-\!O\!\right)_n\!\!-H$.

This produced a strong ν_{C-O-C} antisymmetric mode peak at 1120 cm^{-1} and a medium-strength symmetrical mode peak at 1061 cm^{-1}. In polypropylene

$$\left(\!CH_2\!-\!\underset{\underset{CH_3}{|}}{CH}\!-\!O\!\right)_n$$
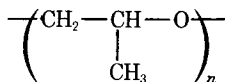
oxide, four bands are observed, at 1138, 1100, and 1012 cm^{-1}. Evidence of the development of a fourth peak is furnished by the variable behavior of the 1105 cm^{-1} peak. This was assigned primarily to a phthalic anhydride aromatic δ_{C-H} mode; but its optical density behavior during cure exhibited a minimum, suggesting additional peak formation. Unfortunately, the information available for branched ethers and polyethers is insufficient to specify the nature of the ether linkages produced.

The 1038 and 1010 cm^{-1} peaks remain constant during cure and assigned to aromatic δ_{C-H} modes are discussed above, with the former containing aromatic alkyl ν_{C-O} contributions. Two weak peaks at 990 and 960 cm^{-1} develop in parallel during cure. These are most readily assigned to ester γ-skeletal modes. In contrast, the other weak peak at 936 cm^{-1} remains virtually unchanged. This peak was weakly present in unreacted CT200 but was unassigned.

The epoxide group deformation mode peak at 915 cm^{-1} in the unreacted resin is swamped by the phthalic anhydride γ_{C-O} mode peak at 900 cm^{-1} which decreased during cure. The epoxide group should exhibit a second peak at 840 to 870 cm^{-1}. The peak at 862 cm^{-1} disappeared during cure and was also assigned to an epoxide ring deformation mode. Unfortunately, it was too weak to follow in detail.

The peak at 830 cm^{-1} is well defined, forming a useful low-wave number reference because it does not change during cure and is assigned to the resin aromatic δ_{C-H} (out-of-plane deformation). Weak contributions to the wings may come from δ_{-CH_2} rocking modes and resin $C(CH_3)_2$ skeletal vibrations which contribute to the 810 cm^{-1} region.

Assignment of the remaining low-frequency peaks is unclear except for the 712 and 534 cm^{-1} peaks, which are assigned to phthalic anhydride γ_{C-H} and $\gamma_{(C-C-C)}$ modes, respectively. In this region, a peak at 740 cm^{-1} appears during

TABLE IV
nth-Order Rate Equations and Corresponding Reaction Extent (p) Integral Equations

Order	Rate equation	Integral equation
0	$\dfrac{dc}{dt} = k$	$c_0 k_t = p$
$\dfrac{1}{2}$	$\dfrac{dc}{dt} = kc^{1/2}$	$c_0^{1/2} kt = (1 - P)^{1/2} - 1$
1	$\dfrac{dc}{dt} = kc$	$kt = \ln (1 - P)^{-1}$
2	$\dfrac{dc}{dt} = kc^2$	$c_0 kt = \dfrac{P}{(1 - P)}$
3	$\dfrac{dc}{dt} = kc^3$	$2c_0^2 kt = (1 - P)^{-2} - 1$

cure. As discussed later, its increase parallels that of the 1725 cm^{-1} aromatic ester $\nu_{C=O}$ peak, which contains both monoester and diester contributions. A low-frequency skeletal mode is likely, but its exact identity is unknown.

OPTICAL DENSITY KINETICS OF CURE

Analogous to the reaction extent defined by Flory,[22] an optical density extent of reaction may be defined:

$$C(t) = [1 - P(t)]C_0 \qquad (17)$$

where $C(t) = D(t) - D(\infty)$. The nth-order rate equations and their corresponding integral equations are tabulated in Table IV. These integral equations allow linearized kinetic plots to be constructed to test the behavior of individual groups during reaction.

Hydroxyl, Epoxide, and Carboxylic Acid Group Behavior

First spectral observations after mixing indicated the presence of associated carboxylic acid species and aromatic ester species. The former's optical density time dependence is illustrated in Figure 2, indicating the $t = 0$ step and subsequent peaked behavior. Consideration of the free hydroxyl absorption peak at 3500 cm^{-1} before and after mixing indicate also a change in optical density from 0.0548 to 0.0503, a change of about 8%. These results suggest an immediate rapid reaction of anhydride and hydroxyl groups on addition of the former and during mixing followed by more continuous behavior. The hydroxyl group optical density remained almost constant during the first 3 h of observation. Subsequent analysis was unreliable due to powder sample artifacts.

The epoxide group optical density could not be followed reliably due to peak weakness or overlap. Inspection of discernible peaks and shoulders (see Tables II and III) suggested that they decrease in line with anhydride consumption.

Phthalic Anhydride

The kinetic behavior of this compound is crucial in differentiating reaction mechanisms. Four reliable peaks were chosen for kinetic analysis and included
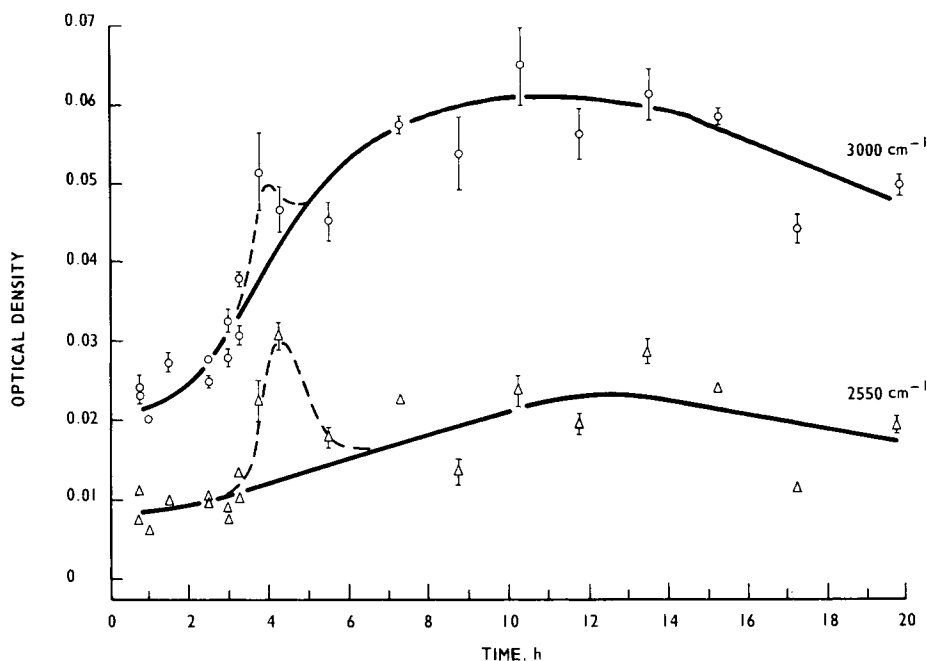
Fig. 2. 3000 and 2550 cm^{-1} carboxylic acid peak optical density variation during reaction of CT200–HT901.

those at 1850, 1772, 900, and 712 cm^{-1}. The optical density time dependence of the 1850 and 712 cm^{-1} peaks is shown in Figure 3. The $D(0)$ values were obtained by extrapolation and the $D(\infty)$ values assessed directly. All peaks exhibited nonzero $D(\infty)$ values consistent with a small quantity of unreacted anhydride.
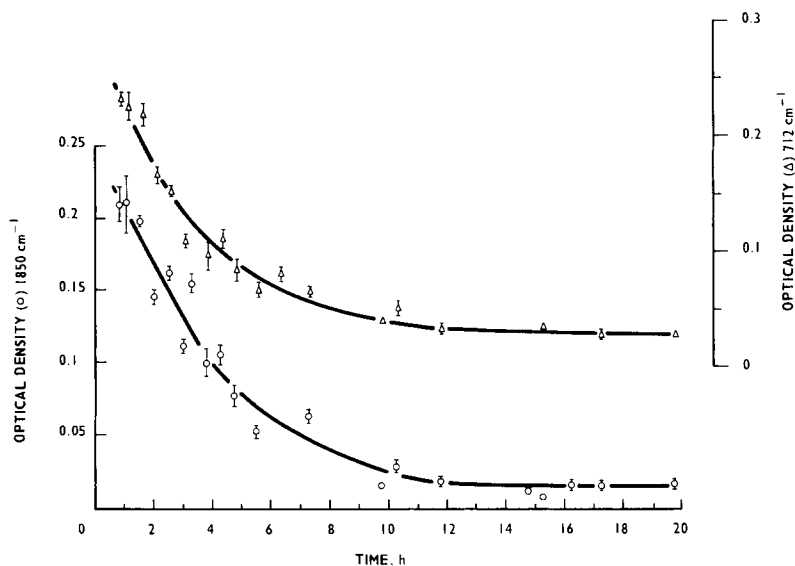

Fig. 3. 1850 and 712 cm^{-1} phthalic anhydride peak optical density variation during reaction of CT200–HT901.
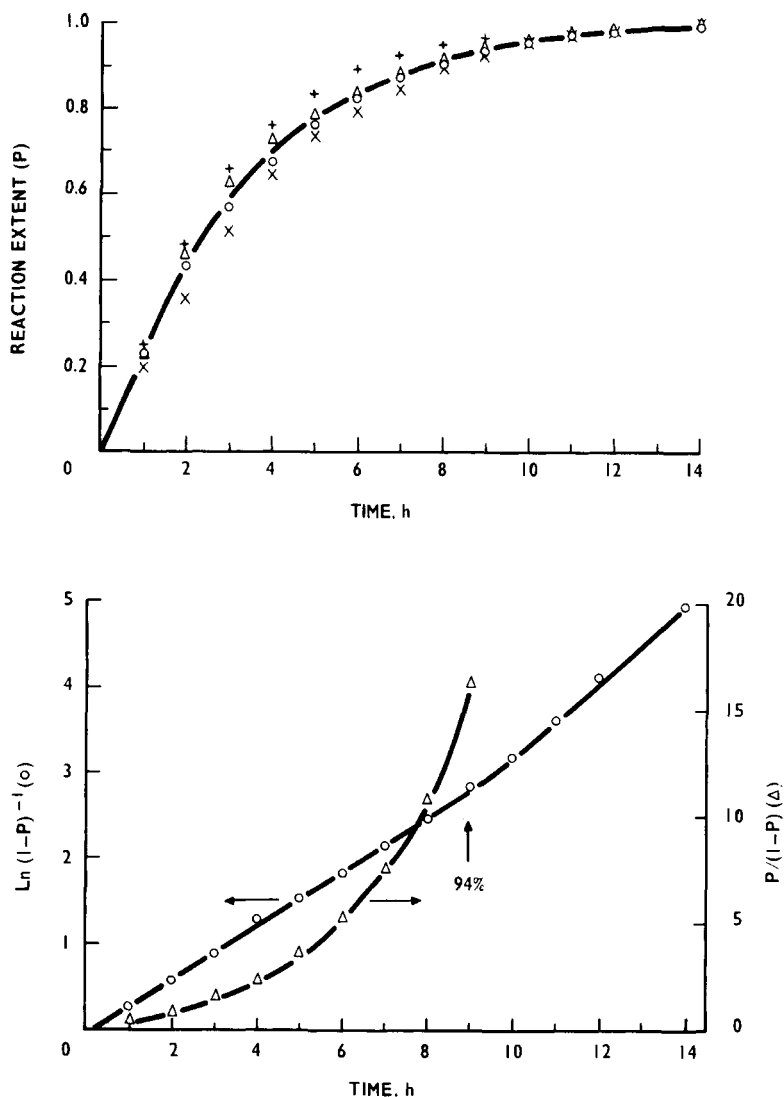
Fig. 4. Phthalic anhydride reaction extent and first- and second-order kinetic plots from smoothed optical density plots: (X) 1850 cm^{-1}; ($\triangle$) 1772 cm^{-1}; (+) 900 cm^{-1}; (O) 712 cm^{-1}.

Reaction extent and resulting linearized kinetic plots are shown in Figure 4, where both first- and second-order kinetics are considered. The behavior is first-order from 20 to 94% of the reaction over the first 9 h of cure. Above 94%, a second first-order-like region is encountered. From the slope of the first-order plot, a rate constant of 8.6×10^{-5} s^{-1} is obtained.

Aromatic Ester

In this case, assessment of the monoester (dicarboxylic acid), diester, and total ester behavior is possible. In this respect, we must assume that the associated carboxylic acid peaks at 3000 and 2550 cm^{-1} include the behavior of any
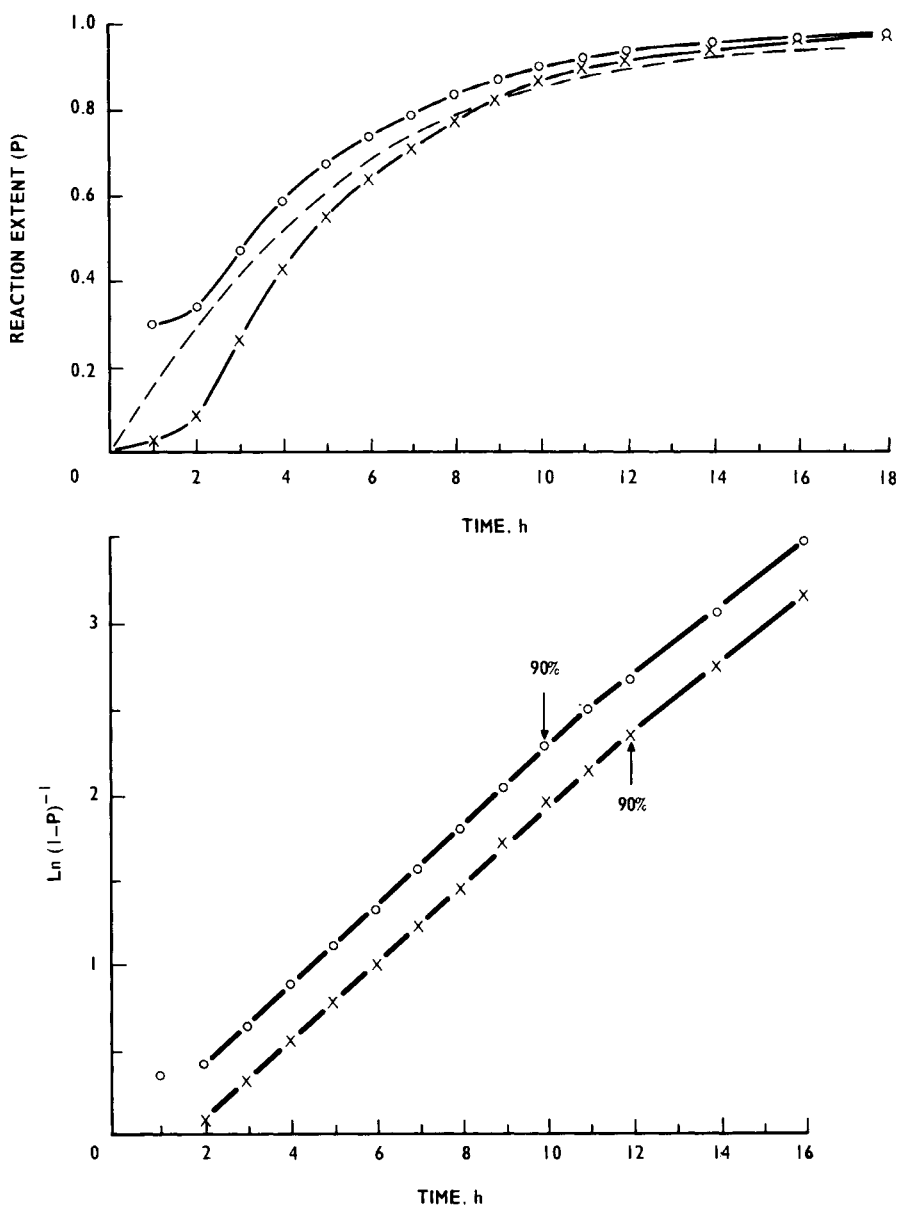
Fig. 5. Total aromatic ester reaction extent and first-order kinetic plots for initial optical density values of 0 and 0.1. The 740 cm^{-1} peak optical density behavior is included for comparison: (- - -) 740 cm^{-1}; (——) 1725 cm^{-1}; (O) D (0) = 0; (×) D (0) = 0.1.

nonassociated moeties as well, because the 1705 cm^{-1} peak is too weak to follow. The total aromatic ester content is contained in the 1725 cm^{-1} peak. In this case, an early rapid reaction contribution is evident in the optical density behavior allowing two options for extent of reaction and kinetic analysis, these being $D(0)$ = 0 and $D(0) \sim 0.1$. Both were considered and are illustrated in Figure 5. Both display first-order kinetics which in the $D(0)$ = 0 case cover the reaction range 24 to 90%, and in the $D(0)$ = 0.1 case cover the range 10 to 90%; the corresponding
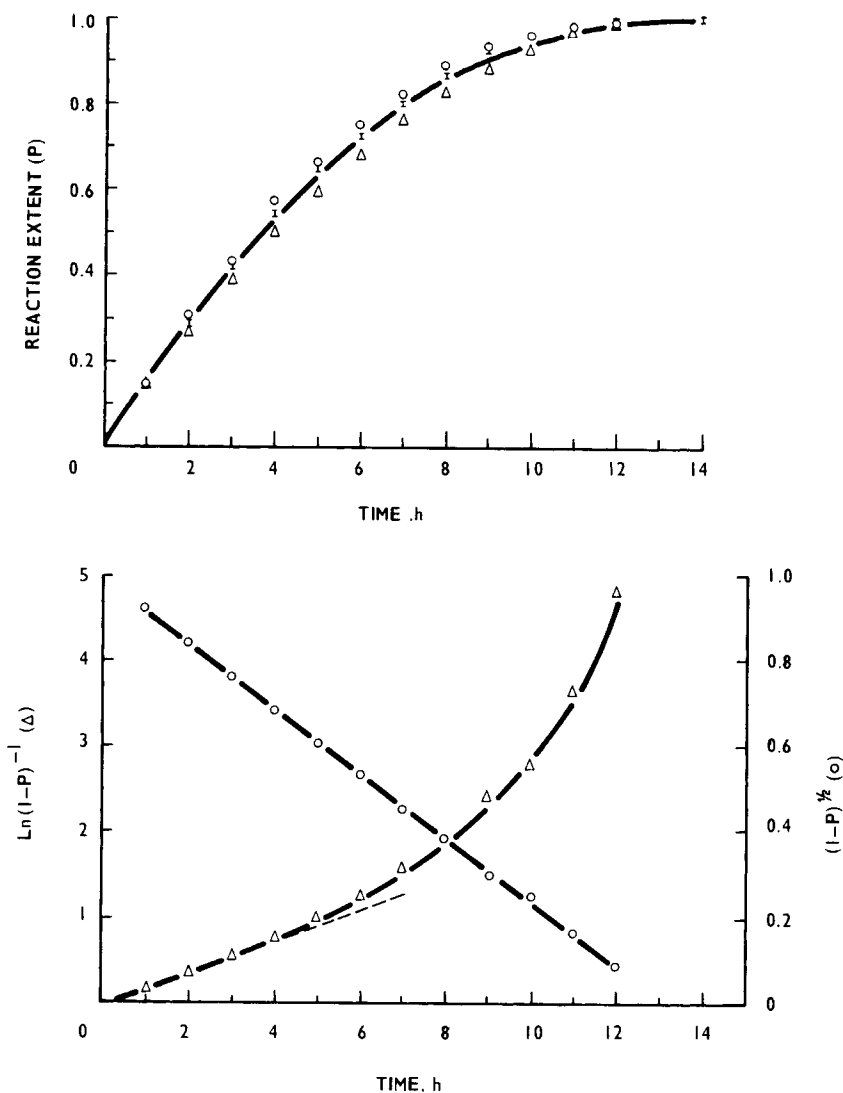
Fig. 6. Branched ether reaction extent and first- and half-order kinetic plots: (I) 1068 cm^{-1}; (O) 1120 cm^{-1}; (△) 1140 cm^{-1}.

rate constants are 6.5 and 6.2 × 10^{-5} s^{-1}, respectively. The assignment of the 740 cm^{-1} peak was unclear. Its reaction behavior is shown in Figure 7 to be similar to the 1725 cm^{-1} behavior; it displayed first-order kinetics up to about 80% with a slightly slower rate constant of 5.6 × 10^{-5} s^{-1}.

The 990 and 960 cm^{-1} peaks were tentatively assigned to ester γ-skeletal modes. Their behavior is similar and typified by the 990 cm^{-1} reaction extent shown in Figure 7. This S-shaped behavior and the carboxylic acid peak behavior is typical of the three-phase consecutive first-order reaction situation discussed above. This suggests that the behavior of the 990 cm^{-1} peak is representative of diester or polyester formation as distinct from monoester or total ester formation.
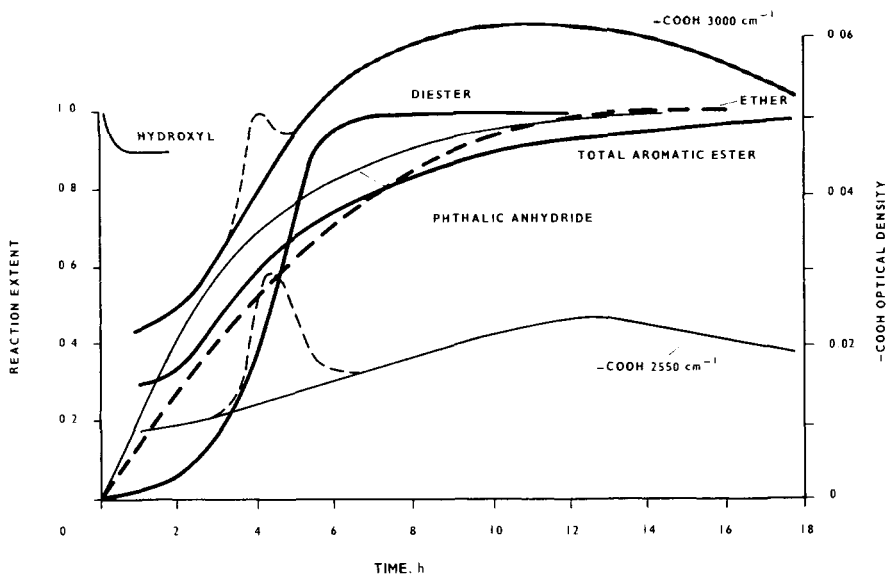
Fig. 7. Summary of the reaction kinetics of CT200–HT901 during reaction at 125°C.

Branched Ether

The assigned branched ether peaks at 1140, 1120, and 1068 cm^{-1} display the optical density behavior summarized in Figure 7. In all cases, linear extrapolation was used to obtain $D(0)$ values and the resulting extent of reaction and kinetic linearization plots are shown in Figure 6. In this case, half-order kinetics is applicable over the whole reaction. However, a first-order kinetic fit may be applicable to the initial 50% of the reaction. For comparison purposes, the initial first-order behavior rate constant is about 5×10^{-5} s^{-1}.

DISCUSSION

The overall infrared reaction behavior is summarized in Figure 7, where the indicated distinctions between monoester, diester (and polyesters), and total aromatic ester are assumed correct. Generally, significant hydrogen bonding occurs between epoxide and hydroxyl groups before and during reaction and between carboxylic acid components during cure, which is probably intermolecular dimerlike in origin.

The following reaction events are interpretable best in terms of the step addition reactions (1) to (3) and the further reaction structures of eqs. (14) to (16), albeit that the detailed reaction behavior is governed by the properties of the reacting phase as discussed later. The overall reaction extent may be conveniently referred to that of the phthalic anhydride. Initial addition of phthalic anhydride results in its rapid reaction with available hydroxyl groups forming a reservoir of carboxylic acid groups. About 8% of the total hydroxyl group number is involved, and light scattering results to be reported suggest that it is an immediate step change. This may result from the initial high temperature of mixing, which is about 10°C above the required cure temperature, or an availability of more highly reactive hydroxyl groups or hydroxyl regions. The

TABLE V
Comparison of the CT200–HT901 Infrared Kinetic Behavior and that of the Fisch and Hofman
(F.H.) Araldite B–Phthalic Anhydride System

Chemical species	Reaction order	Rate constant, $\times 10^{-5}$ s^{-1}
Phthalic anhydride		
Infrared	1	8.6
F.H.	1	14
Total aromatic ester		
Infrared	1	6.5
Diester F.H. (inferred)	1	7.9
Ether		
Infrared	½(1)	(5)
F.H. (inferred)	1	12

carboxylic acid reservoir continues to grow, slowly at first before continuous first-order reaction consumption of anhydride occurs. This acts to allow etherification reactions to proceed and locally conserve the free hydroxyl concentration. Ether formation continues with half-order kinetics. The diester crosslinking reaction rate increases nonsimply until it is very rapid after 20 to 30% anhydride consumption. At this stage, the carboxylic acid group data suggest an early peaked behavior. Unfortunately, the data of Figure 2 is too inaccurate to be decisive. However, such peaked behavior coincident with the diester rapid reaction rate region is consistent with that expected from consecutive-step reactions (1) and (2) as discussed with reference to eq. (11). After 75% anhydride consumption, the diester reaction extent exceeds the ether reaction extent, and at 78% consumption, the diester reaction extent exceeds that of the anhydride, continuing to completion at about 90% anhydride consumption. This implies that at least 10% of the anhydride is present as monoester and unreacted residue.

Functional-group chemical analysis of an Araldite B–PA system cured at 125°C was reported by Fisch and Hofman.[2] The DGEBA resin was similar to CT200 and contained 2.5 epoxide and 2.8 hydroxyl equivalents per kg, and a system reaction stoichiometry of 0.85 anhydride groups per epoxide groups was used. Their results indicate that about 25% of the available anhydride is not involved in diester crosslinking. From their published data, it was possible to construct extent of reaction and kinetic plots the results of which are compared with the infrared results in Table V. Both anhydride consumption reactions proceed with first-order kinetics with the Fisch and Hofmann reaction rate about 1.6 times larger. This could occur due to temperature differences or the greater hydroxyl group concentration of the Fisch and Hofmann resin system. Indeed, the latter exhibits an initial reaction hydroxyl loss of 30%, whereas it is 8% in the system studied here, which had residual volatiles removed prior to reaction. In fact, the similar epoxide group equivalents of the two systems could imply hydroxyl-containing impurities in the Fisch and Hofmann system which would act to accelerate anhydride consumption. The Fisch and Hofmann data indicate that phthalic anhydride, diester, and ether reactions proceed with first-order kinetics (k_1, k_2, and k_3, respectively) with

$$k_1 \sim k_3 > k_2 \text{ and } k_1/k_2 \sim 1.6$$

The infrared study indicates first-order phthalic anhydride kinetics and half-order ether kinetics with nonsimple esterification such that initially k_3 appears $> k_2$ and

$$k_1 > k_3, \; k_1/k_3 \sim 1.3$$

But overall, after the esterification induction period, $k_2 > k_3$.

Neither study supports the termolecular reaction schemes of Tanaka and Kakiuchi which negate the etherification reaction. However, the obvious occurrence of hydrogen-bonded complexes may favor activated complexes similar to those proposed by Tanaka and Kakiuchi.

Hydroxyl group nonavailability or restriction appears the most likely cause of anhydride first-order kinetics. This could occur in several ways: steric hindrance, trapping in molecular aggregates, formation of reaction nuclei exhibiting reduced mobility, or diffusion-limited reactions generally. In these epoxy systems, the reacting components are their own solvent, and the reacting phase has high viscosity which increases as reaction proceeds (from 1 poise to 100 poise in the first 3 h) eventually becoming a viscoelastic crosslinked solid above the high-temperature physical gel point.

Waite[23] considered a general theory of bimolecular reaction rates in liquid and condensed phases. For both, he showed that for $X + Y \rightarrow XY$, the reaction is second-order if the barrier for reaction upon collision is of the same order as that for diffusion; whereas for $X + Y \rightarrow Y$ (a colloidal or reaction nuclei situation), it will be first-order after times long compared to r_0^2/D, where r_0 is a capture radius and the joint diffusion constant $D = D_X + D_Y$. In condensed phases, where $X + Y \rightarrow XY$ is limited by diffusion, the rate is still second-order, but the rate constant will be time and viscosity dependent becoming constant after some fixed transition period. These statements assume a constant activation energy on collision. This suggests that colloidal reactions or hydroxyl restriction, rather than high viscosity, will lead to consistent first-order reaction behavior when the functional group reactivity is constant. In these epoxy systems, the hydroxyl groups would be retained in the colloid or aggregate particle Y. This is consistent with strong hydroxyl–epoxide hydrogen bonding in the unreacted resin and light scattering observations[1] (to be reported) which indicate the presence of molecular aggregates prior to reaction. It then follows that aggregate formation is hydroxyl group dependent and aggregates contain a higher hydroxyl group content than the surrounding matrix and have a higher probability for anhydride (and other) reactions to initiate inhomogeneous reaction. A variety of light scattering studies and fracture surface observations, which reveal changing heterogeneity, support this model. The application of this model to a high epoxide/hydroxyl-group ratio epoxy system is discussed in the following report.

CONCLUSIONS

The bisphenol A epoxy resin–phthalic anhydride system studied, chemically reacts by consecutive-step addition esterification involving carboxylic acid group intermediates and simultaneous addition etherification, in agreement with the basic reactions proposed by Fisch and Hofmann. However, epoxide–hydroxyl and carboxylic acid–dimer hydrogen bonding occurs during reaction. No evidence was found to support the termolecular reaction schemes proposed by Tanaka and Kakiuchi.

STEVENS

Phthalic anhydride consumption and total aromatic ester formation follow first-order kinetics. Diester formation follows S-shaped kinetics, and branched ether formation generally follows half-order kinetics. Carboxylic acid formation occurs rapidly on initial component mixing involving consumption of about 8% of the available hydroxyl groups. Subsequent formation follows that expected of a consecutive-step reaction intermediate. At least 10% of the available anhydride is incompletely esterified.

The observations support a hydroxyl group-limited colloidal type inhomogeneous reaction mechanism.

References

1. G. C. Stevens, J. V. Champion, P. Liddell, and A. Dandridge, *Chem. Phys. Lett.*, **71**(1), 104 (1980).

2. W. Fisch and W. Hofmann, *J. Polym. Sci.*, **XII**, 497 (1954); *Makromol. Chem.*, **54–56**, 8 (1961); *Plast. Technol.*, **7**, 28 (1961); see also W. Fisch, W. Hofmann, and K. Koskikallio, *J. Appl. Chem.*, 429 (1956); W. Fisch, W. Hofmann, and R. Schmid, *J. Appl. Polym. Sci.*, **13**, 295 (1969).

3. Y. Tanaka and H. Kakiuchi, *J. Appl. Polym. Sci.*, **7**, 1063 (1963); *ibid.*, **7**, 1951 (1963); *J. Polym. Sci., Part A*, **2**, 3405 (1964).

4. H. Lee and K. Neville, *Handbook of Epoxy Resins*, McGraw-Hill, New York, 1967.

5. Y. Tanaka and T. F. Mika, in *Epoxy Resins: Chemistry and Technology*, C. A. May and Y. Tanaka, Eds., Marcel Dekker, New York, 1973.

6. H. Batzer and S. A. Zahir, *J. Appl. Polym. Sci.*, **19**, 585 (1975).

7. E. C. Dearborn, R. M. Fuoss, and A. F. White, *J. Polym. Sci.*, **16**, 201 (1955).

8. R. F. Fischer, *J. Polym. Sci.*, **XLIV**, 155 (1960).

9. L. Shechter and J. Wynstra, *Ind. Eng. Chem.*, **48**, 86 (1956).

10. H. Mark and R. Raff, *High Polymeric Reactions, Their Theory and Practice*, Interscience, New York, 1941.

11. K. E. Lüttgert and R. Bonart, *Colloid Polym. Sci.*, **254**, 310 (1976).

(12) C. N. R. Rao, *Chemical Applications of Infrared Spectroscopy*, Academic Press, New York, 1963.

13. R. G. J. Miller and H. Willis, Eds., *Infrared Structural Correlation Tables*, Eds., Heyden, London.

14. Y. Hase, C. U. Davanzo, K. Kawai, and O. Sala, *J. Molec. Struct.*, **30**, 37 (1976).

15. P. V. Sidyakin, V. L. Karpov, B. N. Yegorov, and Z. S. Yegorova, *Vysokomol. Soedin.*, **A13**(10), 2195 (1971); Translated in *Polym. Sci. USSR*, **13**(10), 2464 (1971).

16. P. V. Sidyakin, *Vysokomol. Soedin.*, **A14**(5), 969 (1972); Translated in *Polym. Sci. USSR*, **14**(5), 1087 (1972).

17. P. Eyerer, *J. Appl. Polym. Sci.*, **18**, 975 (1974).

18. L. I. Komarova, S. N. Salazkin, I. A. Bulgakova, M. I. Malaniya, S. V. Vinogradova, and V. V. Korshak, *J. Polym. Sci. Polym. Chem. Ed.*, **16**, 1643 (1978).

19. D. Patterson and I. M. Ward, *Trans. Farad. Soc.*, **53**, 291 (1957).

20. I. M. Ward, *Trans. Farad. Soc.*, **53**, 1406 (1957).

21. W. H. T. Davison, *J. Chem. Soc.*, 3270 (1955).

22. P. J. Flory, *Principles of Polymer Chemistry*, Cornell University Press, New York, 1967.

23. T. R. Waite, *Phys. Rev.*, **107**(2), 463 (1957); *J. Chem. Phys.*, **28**(1) 103 (1958).